Neuro-Oncology Advances
5(1), 1–12, 2023 | https://doi.org/10.1093/noajnl/vdad082 | Advance Access date 7 July 2023

Spectral flow cytometry identifies distinct nonneoplastic plasma extracellular vesicle phenotype in glioblastoma patients

Abudumijiti (Zack) Aibaidula, Cori E. Fain, Luz Cumba Garcia, Annelise Wier, Samantha M. Bouchal, Megan M. Bauman, Mi-Yeon Jung, Jann N. Sarkaria, Aaron J. Johnson, Ian F. Parney

Department of Molecular Pharmacology and Experimental Therapeutics, Mayo Clinic Graduate School of Biomedical Sciences, Mayo Clinic, Rochester, Minnesota, USA (A.A.); Department of Neurological Surgery, Mayo Clinic, Rochester, Minnesota, USA (A.A., A.W., S.M.B., M.M.J.B., M.J., I.F.P.); Department of Immunology, Mayo Clinic Graduate School of Biomedical Sciences, Mayo Clinic, Rochester, Minnesota, USA (C.F., L.C.G., A.J.J., I.F.P.); Mayo Clinic Alix School of Medicine, Mayo Clinic, Rochester, Minnesota, USA (S.M.B., M.M.J.B.); Department of Radiation Oncology, Mayo Clinic, Rochester, Minnesota, USA (J.N.S.)

Corresponding Author: Ian F. Parney, MD PhD, Department of Neurological Surgery, Mayo Clinic, 200 First Street SW, Rochester, MN, 55905, USA (Parney.Ian@mayo.edu).

Abstract

Background. Glioblastoma (GBM) is the most common malignant brain tumor and has a poor prognosis. Imaging findings at diagnosis and in response to treatment are nonspecific. Developing noninvasive assays to augment imaging would be helpful. Plasma extracellular vesicles (EVs) are a promising biomarker source for this. Here, we develop spectral flow cytometry techniques that demonstrate differences in bulk plasma EV phenotype between GBM patients and normal donors that could serve as the basis of a liquid biopsy.

Methods. Plasma EVs were stained for EV-associated tetraspanins (CD9/CD63/CD81), markers indicating cell of origin (CD11b/CD31/CD41a/CD45), and actin/phalloidin (to exclude cell debris). EVs were analyzed using spectral flow cytometry. Multiparametric analysis using *t*-distributed stochastic neighbor embedding (t-SNE) and self-organizing maps on flow cytometry data (FlowSOM) was performed comparing GBM and normal donor (ND) plasma EVs.

Results Size exclusion chromatography plus spectral-based flow cytometer threshold settings enriched plasma EVs while minimizing background noise. GBM patients had increased CD9+, CD63+, CD81+, and myeloid-derived (CD11b+) EVs. Multiparametric analysis demonstrated distinct surface marker expression profiles in GBM plasma EVs compared to ND EVs. Fifteen plasma EV sub-populations differing in size and surface marker expression were identified, six enriched in GBM patients and two in normal donors.

Conclusions. Multiparametric analysis demonstrates that GBM patients have a distinct nonneoplastic plasma EV phenotype compared to ND. This simple rapid analysis can be performed without purifying tumor EVs and may serve as the basis of a liquid biopsy.

Key Points

- Spectral flow cytometry rapidly characterizes plasma extracellular vesicles (EVs). Nonneoplastic plasma EVs have a distinct phenotype in GBM patients. Plasma EV flow cytometry is promising for GBM liquid biopsy.

Glioblastoma (GBM, WHO grade IV) is the most common malignant brain tumor in adults.[1,2] Even with maximal safe resection, radiotherapy and adjuvant chemotherapy,[3] median overall survival is just over 15 months[4] and 5-year survival is only 4%.[5] Treatment response is generally assessed clinically and with magnetic resonance imaging (MRI). Unfortunately, inflammatory pseudoprogression with associated clinical symptoms, new contrast enhancement, and edema indistinguishable from true

Importance of the Study

Because glioblastoma imaging findings are nonspecific at both diagnosis and recurrence, developing noninvasive liquid biopsies to augment MRI would be helpful. Plasma extracellular vesicles (EVs) are a promising biomarker source for liquid biopsies. However, EV analysis typically relies on technically demanding methods to separate and concentrate tumor EVs followed by additional RNA/DNA sequencing or proteomics. In this study, we developed spectral flow cytometry techniques enabling analysis of bulk plasma EVs in GBM patients without specifically isolating tumor-derived EVs. Multiparametric analysis demonstrated distinct surface marker expression and size profiles in GBM patients' nonneoplastic plasma EVs compared to normal donors. These findings underscore GBMs systemic effects and demonstrate a novel technique utilizing widely available technology that can potentially identify GBM patients within a few hours based on a blood test without complex EV isolation, genomic, or proteomic steps. With further validation, this rapid technique could be widely applied as a liquid biopsy.

progression is common.[6,7] Differentiating pseudoprogression from true tumor progression is critical to ensure appropriate management decisions but challenging based on clinical findings and MRI alone. Definitive diagnosis can be made via brain biopsy, but this is invasive, carries risk, and may not capture tumor/necrosis heterogeneity.[8] Minimally invasive diagnostic tools to augment clinical and imaging findings in GBM patients are a vital, unmet clinical need.

Extracellular vesicles (EVs) are lipid bilayer-encapsulated nanoparticles released by all cells. They are present in body fluids including plasma, cerebral spinal fluid, and urine. EV size is heterogeneous but has previously been used to categorized EVs as exosomes (30–150 nm), microvesicles (50 nm–1 μm), oncosomes (1–10 um), or apoptotic bodies (500 nm–5 μm), all of which may have unique cargo and biogenesis.[9] EV cargo includes nucleic acids (RNA, DNA), proteins (immunoglobulins, tumor-specific proteins, surface tetraspanins, and enzymes), lipids, and metabolites.[10–16] EV cargo reflects cell of origin, making these nanoparticles attractive candidates for liquid biopsy in glioblastoma.[11] This has typically involved separating/concentrating GBM-derived EVs from body fluids and performing deep sequencing and/or proteomic analysis.

However, GBM patients have higher plasma EV concentrations than healthy individuals. Measuring this one bulk variable can be used for treatment response assessment.[17] Given that GBMs do not generally metastasize and that there are multiple potential cellar sources for plasma EVs (e.g. leukocytes, red blood cells, platelets, endothelial cells), the source of increased plasma EVs in GBM patients remains uncertain. EV flow cytometry is possible and could clarify cells of origin but technical challenges to nanoscale flow cytometry have been a barrier.[18] To address this, we sought to develop a simple but rigorous spectral flow cytometry panel characterizing surface marker expression profiles of GBM patients' plasma EVs in comparison to normal donors as proof of principle that this technique is feasible for liquid biopsies in GBM patients.

Methods

GBM Patient and Normal Donor Blood and Plasma

Primary GBM (IDH wildtype) patient plasma samples were obtained from the Mayo Clinic Neuro-Oncology Biobank (IRB#12005438, #22000883). All GBM plasma samples were collected in the operating room before the surgery. Normal donor plasma samples were obtained from discarded anonymized healthy donor leukoreduction chambers from the institutional blood bank. Blood samples were collected in ethylenediaminetetraacetic acid (EDTA) tubes and were centrifuged twice (2000*g* × 10 min) to remove cells and harvest plasma. Plasma samples were further centrifuged (1500*g* × 10 min, 15000*g* × 10 min) to remove any additional cell debris and platelets. Isolated plasma samples were stored in sterile cryogenic vials (Corning Incorporated No. 430488) at –80°C for the following experiments.

Spectral Flow Cytometry Calibration

A 5-laser Cytek Aurora Flow Cytometer equipped with SPECTROFLO software (Cytek Biosciences Inc, Fremont, CA) was used. ApogeeMix beads (Cat#1527, Apogee Flow Systems, United Kingdom) were used for calibration and acquisition settings were optimized to visualize nanoparticles of varying sizes. Serial dilution of ApogeeMix beads was performed to demonstrate detection of single particles. Comparison was made between side scatter (SSC) and various fluorescent channels to optimize thresholds for nanoparticle acquisition.

Isolating CD14+ Monocyte-derived EVs

Peripheral blood mononuclear cells (PBMC) were obtained from discarded anonymized healthy donor leukoreduction chambers from the institutional blood bank via Ficoll gradient centrifugation (800g ×15 min). CD14+ monocytes were isolated from PBMC with CD14+ magnetic beads (Miltenyi Biotec, San Diego, CA) per manufacturer instructions. CD14+ cells (1×10^6/well) were seeded in 6 well plates (Corning Incorporated; Corning, NY) in RPMI (Corning, Mediatech Inc., Manassas, VA) media with 10% fetal bovine serum (FBS) (Atlanta Biologicals, Flowery Branch, CA) and 1% Penicillin/Streptomycin (PEN) Solution (Sigma–Aldrich, St. Louis, MO) and incubated at 37°C/5%CO_2. After 24 hours, media was replaced with serum-free RMPI and incubated for an additional 72 h. Serum-free media was collected and centrifugated (1200 RPM × 10 min ×2) to remove cells and cell debris. The supernatant was ultracentrifuged at 24000 RPM for 16 h at 4°C (Optima LE-80K

Ultracentrifuge, Beckman Coulter, Indianapolis, IN) using a swinging bucket (SW 55 Ti, Beckman Coulter, Indianapolis, IN). Supernatant except for the last 300 µl was discarded. Nanoparticle tracking analysis (Nanosight) was performed to determine the concentration of enriched EV samples.

Antibodies

Detailed information for all antibodies utilized in flow cytometry and western blot experiments is listed in Supplementary Table 1.

Developing a EV Flow Cytometry Characterization Panel

Initial assay controls were performed using CD14+ monocyte-derived EVs. Phosphate-buffered saline (PBS; 1X, GE Healthcare Life Sciences Hyclone Laboratories, Logan, UT) was passed through a 100 nm filter (Anotop 10, GE Healthcare UK Limited, UK) and degassed. CD14+ monocyte-derived EVs were stained by diluting 20 µl EVs in 80 µl PBS and incubating with 1 µl of anti-CD9 and/or CD11b antibody (1:100 dilution). Assay controls included buffer only (PBS), buffer with reagent (PBS + antibody), single color staining (CD9 or CD11b), and detergent-treated EV staining control (0.2% SDS) per International Society for Extracellular Vescicles (ISEV) guidelines.[18] Serial dilution of CD9-stained EV samples was performed.

Subsequent assay controls were performed with plasma samples. An antibody mix including anti-CD9, CD11b, CD31, CD41a, CD45, CD63, and CD81 antibodies, phalloidin, and Fc blocking buffer (see Supplementary Table 1 for relative volumes) was spun (21,000g for 10 min) to remove antibody aggregates. About 50 µl plasma samples were added to 50 µl antibody mix, then incubated in the dark at room temperature for 60 min. CD9 titration for plasma samples was performed by staining 50 µl plasma sample with different amounts of CD9 antibodies. PBS only, PBS + all antibodies, single color staining, all color staining, and fluorescence minus one (FMO) controls were performed for all markers. Various antibodies with different fluorochromes were available for the same target. We chose strongly fluorescent fluorochromes compatible with our overall panel. Comparison was made between stained plasma samples and PBS + antibody controls to identify antibodies with the highest signal to noise ratio.

Separating and Concentrating Stained EV Samples

We compared differential ultracentrifugation (DU), density gradient ultracentrifugation (DGU), size exclusion chromatography (SEC), and ultrafiltration (UF) methods for separating and concentrating stained EVs while removing unstained antibodies. For DU, stained EVs (100 µl) in 4 ml PBS were ultracentrifuged (100000g × 90 min; Beckman Coulter Optima LE-80K Ultracentrifuge, Rotor SW55Ti). All supernatant was discarded except for the last 200 µl. For DGU, stained EVs (100 µl) in 3 ml PBS were layered on top of 1 ml of 0.971 M sucrose in an ultra-clear ultracentrifugation tube (13*51 mm, Beckman Coulter, Indianapolis, IN), then ultracentrifuged (190000g × 2 h). The EV pellet was re-suspended in PBS (200 µl). For UF, stained EVs (100 µl) in 14 ml of PBS and concentrated to 500 µl with concentration filters (Amicon Ultra-15, 10 kDa MWCO, Sigma–Aldrich, St. Louis, MO). For SEC, stained EVs (100 µl) were run through qEV single/70 nm columns (IZON Science, Portland, OR). EV fractions were collected per manufacturer's instructions. Purified samples were analyzed on a Cytek flow cytometer with stopping criteria set as a 20 µl sample collection and a SSC-500 threshold. For each method, PBS + Antibody was used as a process control. Finally, SEC to separate/concentrate stained EVs was further tested in plasma samples.

Nanoparticle Tracking Analysis

Particle concentration in cell culture-derived EVs and stained plasma EVs were analyzed using NanoSight (Malverin Panalytical, NanoSight NS300, Westborough MA). Plasma samples were diluted 1:50 and cell culture-derived EVs were diluted 1:100 in filtered PBS prior to NTA. Triplicate measurements (collection time 30 s/each; camera level 15) were analyzed using NTA software (Malvern Panalytical, Westborough MA, Version number MAN0545-01-EN-00) with a threshold of 5.

Western Blots

Samples were prepared with RIPA buffer (50 mM Tris [pH 7.4], 1% Triton X100, 0.25% Sodium deoxycholate, 150 mM NaCl, 1 mM EDTA [pH 8] and 10 mM NaF). Proteins were separated by electrophoresis on SDS-PAGE, followed by membrane transfer and probing with primary antibodies (CD9, CD81, CD63). Secondary antibodies were horseradish peroxidase-conjugated goat anti-rabbit or goat anti-mouse. Membranes were visualized by enhanced chemiluminescence.

Flow Cytometry Data Acquisition and Analysis

After performing daily quality controls, the flow cytometer was cleaned with 10% bleach followed by molecular grade water and filtered PBS at low speed (10 min each). Stained, purified plasma EV samples (20 µl) diluted in 1 mL filtered PBS and then analyzed. EV data were collected on the Cytek Aurora flow cytometer with a SSC-500 threshold and a 100 µl stopping criteria for sample collection. Subsequently, thresholds were changed to the fluorescent intensity peak channels for each fluorophore (V7/B2/YG1/YG5/YG9/R2/R7-600). At least 8×10^4 CD9+ events were collected. Events were manually gated to exclude background noise and only events in the EV size range (gated as "EV region") were included. Flow data was analyzed in FlowJo Software for Windows Version 10.8.1 (FlowJo LLC; Ashland, OR). Further gating for CD9+/phalloidin- events was performed. Finally, we performed self-organizing map clustering via the FlowSOM algorithm and dimensionality reduction using t-distributed stochastic neighbor embedding (tSNE)[19] on a

combined data set. This combined data set contained 8×10^4 randomly sampled phalloidin-negative events from each replicate (n = 10 each for GBM and normal donors). tSNE and subsequent FlowSOM analysis incorporated SSC-A, CD9, CD31, CD11b, CD45, CD41a, CD63, and CD81. Meta clustering was further applied to these samples and an additional 10 GBM and 10 ND replicates (n = 20 total replicates/condition) to determine the frequency of each cluster.

Tumor Volume Assessment

DICOM images from axial T1 post-contrast MRI sequences were imported into 3D Slicer software.[20] Regions of interest outlining contrast-enhancing tumor (excluding necrotic core) and total tumor (enhancement plus necrotic core) were manually created on each slice showing tumor and volumes were calculated using this software.

Statistical Analysis

Student t-test (parametric) and Mann–Whitney test (nonparametric) were used to compare two groups. Statistical significance was determined at $p < 0.05$. p values were adjusted for multiple comparisons and denoted as asterisks: *$p < 0.05$, **$p < 0.01$, ***$p < 0.001$, ****$p < 0.0001$. All data were analyzed and plotted in GraphPad Prism version 9.2.0 for Windows (GraphPad Software, San Diego, CA).

Results

Patients and Normal Donors

A total of 20 GBM patient and 20 ND plasma samples were analyzed. Age and gender of all cases are listed in Supplementary Table 2. Mean age between GBM patients and ND was not significantly different (63.6 ± 8.1 years versus 62.6 ± 8.8 years; $p = 0.71$). Gender was not significantly different between GBM patients and ND ($p = 0.17$).

Optimizing Spectral Flow Cytometry for Nanoparticle Analysis

ApogeeMix calibration beads including fluorescent polystyrene beads (80 nm, 110 nm, 500 nm) and nonfluorescent silica beads (180 nm, 240 nm, 300 nm, 590 nm, 880 nm, 1300 nm) were used to define acquisition parameters for single nanoparticle detection appropriate for EVs. An acquisition threshold of SSC-500 proved optimal for these beads compared to other channel gates (Supplementary Figure 1) and allowed resolution of various distinct sizes (Figure 1B) though the 80 nm and 110 nm fluorescent beads overlapped as a single population. Analysis of 110 nm fluorescent or 880 nm nonfluorescent beads showed linear correlation between serial dilution factor and events detected (R^2 = 0.99) compatible with the detection of single particles (Figure 1C). Optimal data acquisition settings for gain were FSC 20, SSC 1000, SSC-B 1000. Similar analysis using an ImageStreamX MkII Imaging Flow Cytometer (Amnis Corporation; Seattle, WA) demonstrated individual particles but had poor resolution for nonfluorescent beads (Supplementary Figure 2).

Developing an EV Staining Protocol

Since plasma contains heterogeneous particle populations in which the EV concentration remains largely unknown, we first developed our EV staining protocol *in vitro* with monocyte-derived EVs and single color staining for CD9 and CD11b (Figure 1D). Nanoparticle tracking confirmed the presence of EVs and while western blot demonstrated EV-associated tetraspanin (CD9, CD63, CD81), CD11b, and HSP-90 expression (Supplementary Figure 3). There was a small false positive signal in PBS + Ab controls that was not eliminated by 0.2% SDS. However, false positive frequency was much lower than true positive events (CD9: 0.15% vs 9.4%; CD11b: 0.009% vs 1.01%). Exposure to detergent (0.2% SDS) eliminated most of positive events, indicating the vesicular nature of detected particles. Dual color CD9 and CD11 staining showed the majority of CD11b positive events were also positive for CD9 though there were many CD11b–/CD9+ events as well (Figure 1E). There was a linear relationship between dilution factor and CD9+ events suggesting detection of single events (R^2 = 0.99) (Figure 1F). Finally, we further compared antibodies with different fluorochromes for a given surface marker to maximize signal to noise ratio (Supplementary Figure 4).

Indeterminate EV Identification Using Membrane Dyes

Initially, the membrane fluorescence dye PKH67 (Sigma–Aldrich, St. Louis, MO) was tested as a universal EV marker (Supplementary Figure 5). This showed low false positive events in reagent-only controls and increased positive events when EVs were added that were substantially reduced by 0.2% SDS treatment, suggesting a vesicular nature to the positive events. However, two-color staining with PKH67 and various surface markers (CD11b, CD41a, CD45, CD31) was less conclusive. There was a significant increase in corresponding positive events for each surface marker in each single-color staining compared to antibody-alone controls but adding PKH67 dye for double color staining showed few double positive events. The order in which EVs were stained (PKH67 first or surface marker staining first) made no difference to this (data not shown). Treating double-stained EVs with SDS eliminated most of the surface marker-positive and PKH67-positive events. This could indicate PKH67 stains both EV particles and non-EV particles in the plasma. Thus, we discontinued staining with PKH67 as a universal plasma EV labeling strategy and used anti-tetraspanin antibodies (CD9/CD63/CD81) in all subsequent experiments.

Size Exclusion Chromatography is Most Efficient for Separating and Concentrating Stained Plasma EVs

We compared four standard methods for EV separation and concentration: differential ultracentrifugation,

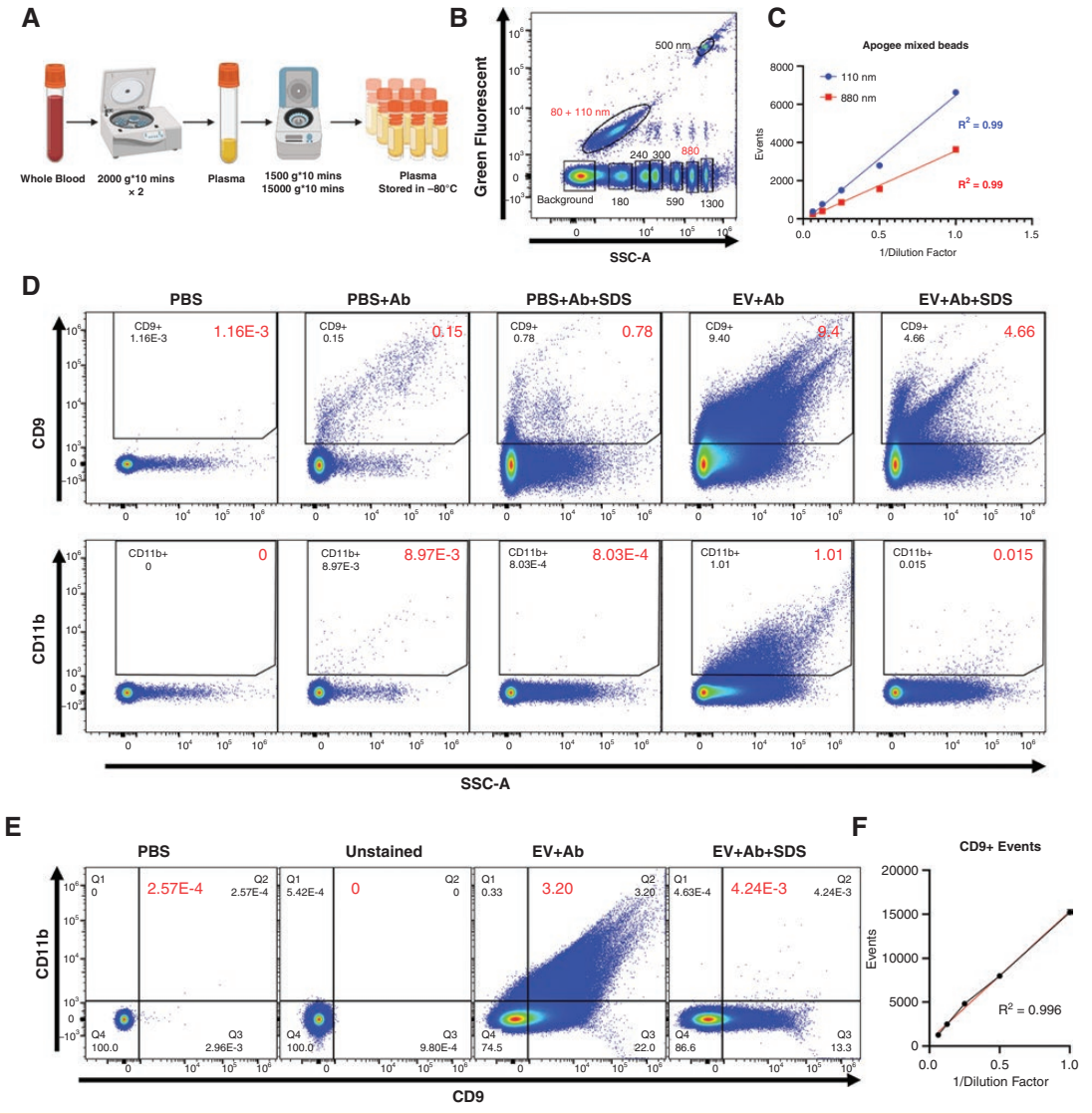

Figure 1 Human plasma processing and EV staining assay controls. (**A**) Schematic showing method for plasma isolation from whole blood. (**B**) Settings of Cytek Aurora Flow cytometer were optimized to visualize different sizes of fluorescent and non-fluorescent ApogeeMix beads. (**C**) Serial dilution demonstrates a linear relationship between dilution and detected events for fluorescent beads (110 nm) and non-fluorescent beads (880nm), suggesting **D, E** clumping is absent. (**D**) EVs isolated from CD14+ monocytes *in vitro* were stained with CD9 (upper panel), CD11b (lower panel), and (**E**) CD9/CD11b together. Controls included buffer-only (PBS), buffer with reagent (PBS+Ab), single color-stained EVs (EV+Ab) and stained but detergent-treated EV samples (EV+Ab+SDS) (**D, E**). Serial dilution of CD9-stained EVs also demonstrated a linear relationship between dilution and detected events.

ultrafiltration, size-exclusion chromatography, density gradient ultracentrifugation (Figure 2). PBS+CD9 antibody was used as a control with each method. Differential ultracentrifugation not only removed most false-positive events (1.08% vs 0.11%) but also reduced the percentage of CD9+ EVs (3.82% vs 0.51%). Ultrafiltration and DGU purification enriched both CD9+ EVs (9.55% vs 3.82%, 8.74% vs 3.82%, respectively) and false-positive events (5.17% vs 1.08%, 5.18% vs 1.08%, respectively). SEC produced the highest signal-to-noise ratio (8.91% vs 0.34%). Furthermore, while all four methods lowered the total yield of CD9+ EVs, this reduction was smallest for size exclusion chromatography (along with ultrafiltration). Repeated experiments comparing separation and concentration efficiency for these four methods using EVs stained for a different surface marker (CD11b) also showed that SEC-purified samples had the highest signal-to-noise ratio (0.95% vs 0.009%) with relatively preserved yield (Supplementary Figure 6). We thus selected SEC as a purification method for our downstream plasma sample staining.

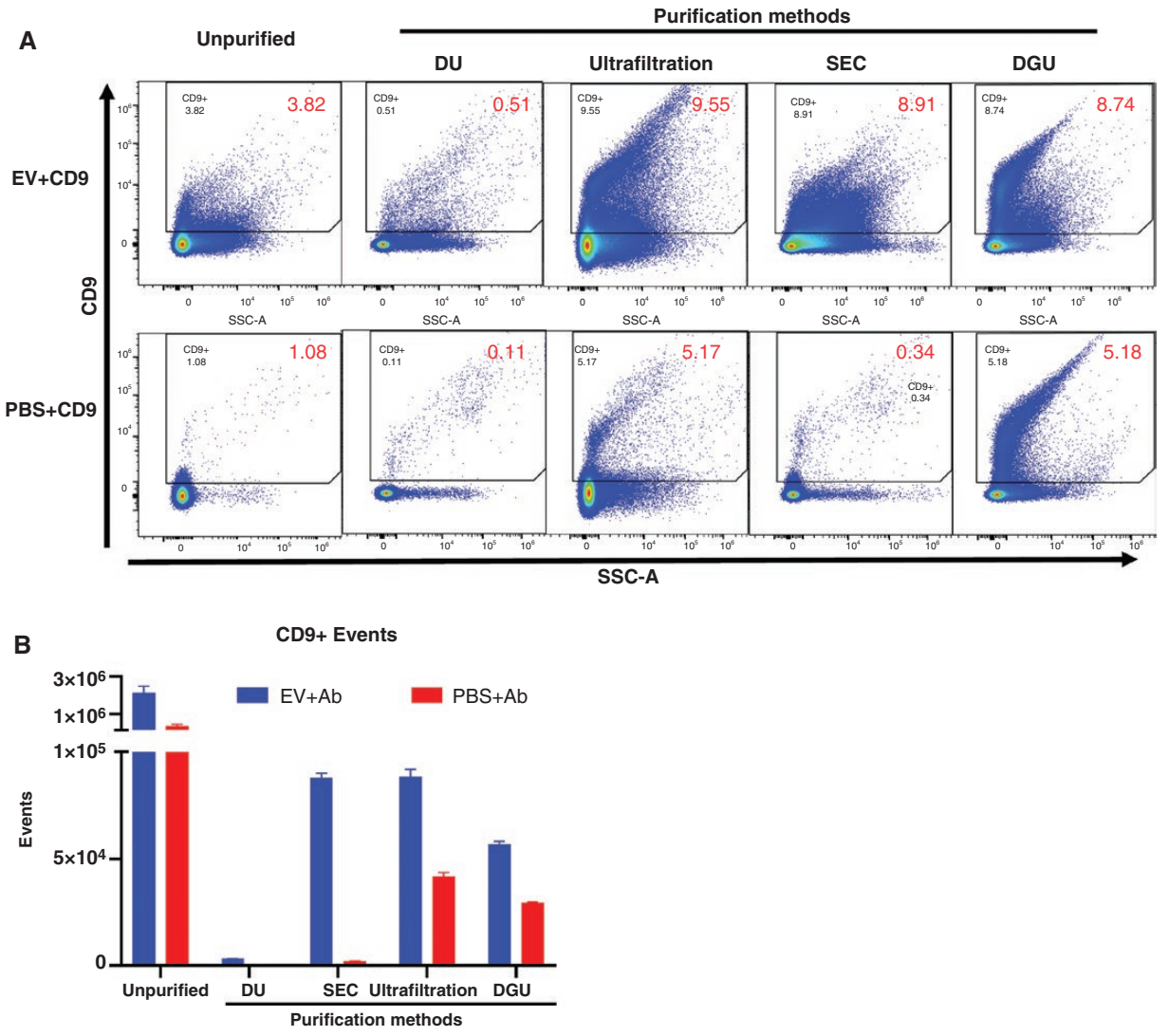

Figure 2 Comparing methods to separate and concentrate stained EVs from unbound antibodies. (**A**) Representative dot plots for CD9-stained EVs from CD14+ monocytes *in vitro* without removing unbound antibodies compared to after differential ultracentrifugation (DU), ultrafiltration, size exclusion chromatography (SEC), or density gradient ultracentrifugation (DGU) to eliminate excess antibodies. PBS+ CD9 antibodies were used as process control (lower panel). (**B**) All four methods reduced EV yield, but SEC was most effective at separating/concentrating EVs with the highest signal-to-noise ratio.

Developing a Staining Panel for Plasma EV Flow Cytometry Analysis

Our protocol for plasma EV staining followed by SEC for EV separation and concentration is shown in Figure 3A. In addition to EV-associated tetraspanins (CD9, CD83, CD81), we sought to identify EVs originating from myeloid cells (CD11b+), leukocytes (CD45+), platelets (CD31+/CD41a+), and endothelial cells (CD31+/CD41a–) and to exclude particles staining for actin (phalloidin+) which represent cellular debris. Antibody titration was performed for the various staining antibodies to demonstrate the lowest amount of antibody that reliably produced similar event rates and mean fluorescence intensity (MFI) (Figure 3B, C). Assay controls for each marker included PBS alone, PBS + antibody, EVs + single antibody, EVs + all antibodies, and EVs + all antibodies except the stain of interest (fluorescence minus one or FMO). These clearly delineated EVs with different surface marker expressions (Figure 3D). CD9 and CD41a were the most abundantly expressed surface markers in plasma EVs identified by our panel. However, most EV-sized particles detected in plasma with our initial SSC-500 threshold for acquisition did not express any surface makers and likely represented contaminating non-EV particles. To minimize this, different data acquisition thresholds were assessed. We had initially chosen an SSC-500 acquisition threshold as our assays with microbead showed this enabled detection of both the fluorescent and nonfluorescent beads while thresholds based on fluorescent spectra only detected fluorescent beads (Supplementary Figure 1). However, this was less of an issue with fluorescently-labeled, SEC-purified plasma EVs

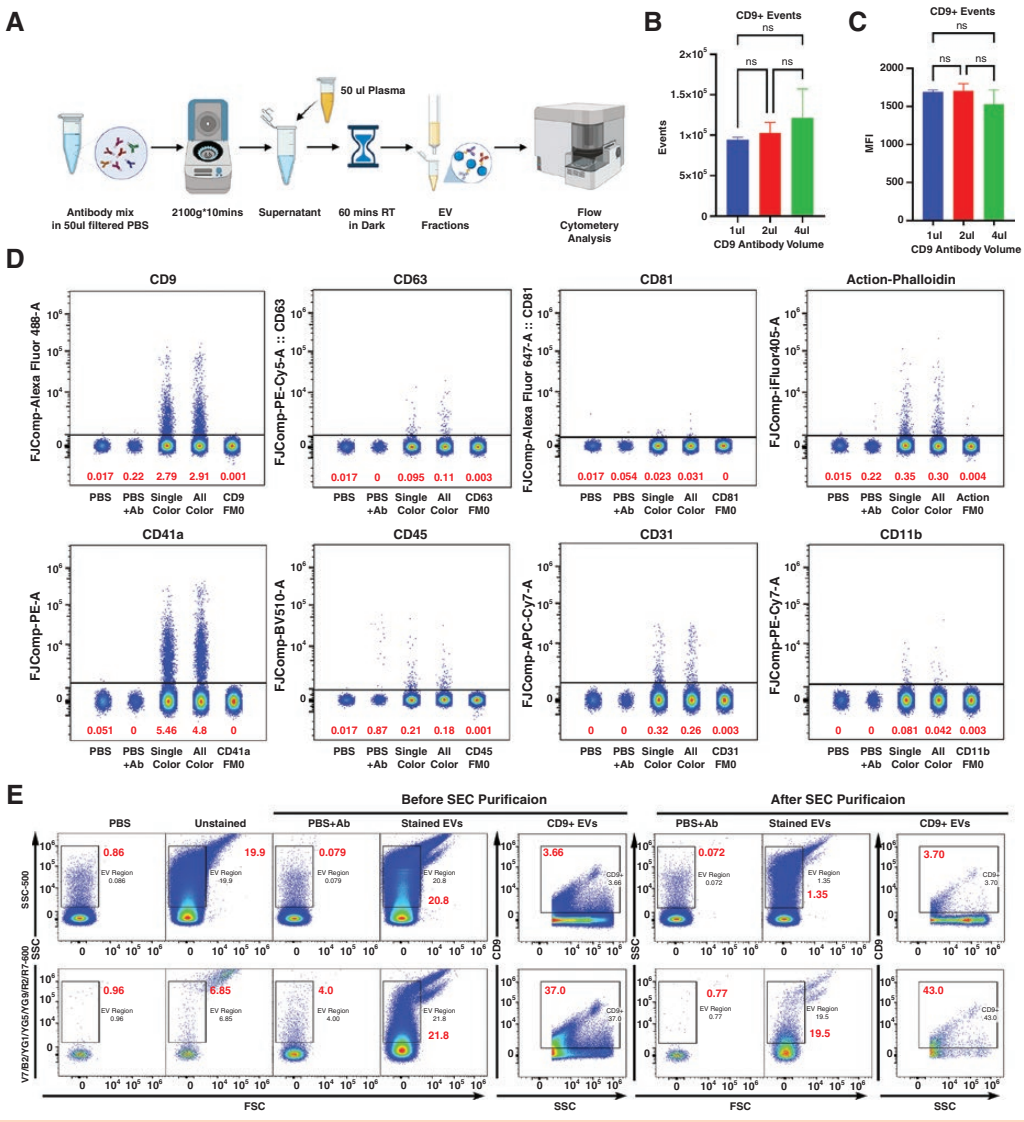

Figure 3 EV staining panel, assay controls, and data acquisition for plasma EV analysis. (**A**) Schematic outlining final staining and separation/concentration methods for plasma EVs. (**B, C**) CD9 antibody titration for plasma EVs samples did not show significant differences in event rates or median fluorescent intensity (MFI) with increasing amounts of CD9 antibodies. (**D**) Representative dot plots showing plasma EV surface marker expression determined using an SSC threshold for EV-associated tetraspanins (CD9, CD63, CD81), phalloidin (staining actin as a marker of contaminating cell debris), and leukocyte/platelet/endothelial markers (CD11b, CD31, CD41a, CD45). Assays controls included buffer only (PBS), buffer with reagents (PBS + all antibodies), single color staining, all color staining, and fluorescence minus one (FMO; all antibodies except one directed against the marker of interest). (**E**). Changing from a size-based SSC threshold for event acquisition (upper panel) to a spectral fluorescence-based surface marker expression threshold (lower panel) markedly reduced non-specific background staining as best demonstrated for CD9 expression in SEC-purified stained EVs. ns = not significant.

where changing from an SSC-500 acquisition threshold to a spectral fluorescence intensity threshold based on all the remaining fluorochromes (V7/B2/YG1/YG5/YG9/R2/R7-600) minimized the detection of both background noise and non-EV particles (Figure 3E).

Analyzing Plasma EVs in GBM Patients and Normal Donors

Only particles in the EV size range were included in our analysis (Figure 4A). Detected particles were further gated for phalloidin-negative events, followed by gating for other surface markers. CD41a+ and CD9+ EVs were the most common phalloidin-negative particles detected in GBM patients and normal donors (Figure 4B). There were no significant differences in CD41a+ EVs (mean 74.04% vs 73.04%, $p = 0.82$), CD31+ EVs (mean 1.14% vs 0.59%, $p = 0.31$) in GBM patients and normal donors. GBM patients trended toward higher CD11b+ EVs (mean 11.29% vs 6.37%, $p = 0.35$) and had significant increases in CD9+ EVs (mean 66.16% vs 24.83%, $p < 0.0001$), CD63+ EVs (mean 9.61% vs 1.99%, $p = 0.014$), and CD81+EVs (mean 6.49%

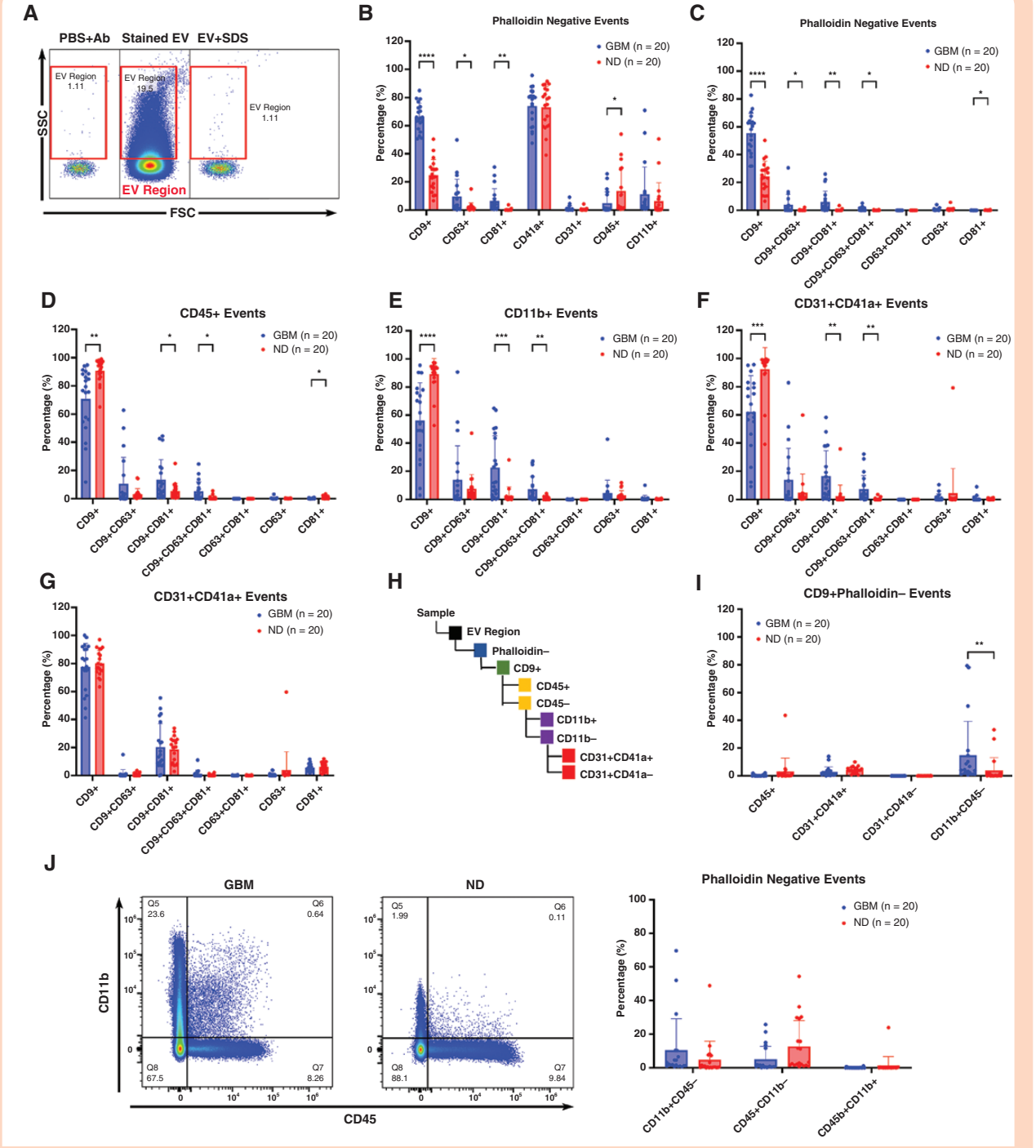

Figure 4 Analysis of plasma EVs in GBM and normal donors. (**A**) Dot plots showing gating strategy and controls for particles in the EV size range (EV region). (**B**) Pooled data from 20 GBM patients and 20 normal donors (ND) showing percentage of EV-associated tetraspanin (CD9, CD63, CD81) and cell of origin (CD45, CD11b, CD31, CD41a) surface marker expression among EV region/phalloidin-negative particles. CD9+ and CD41a+ EVs were most abundant. Tetraspanin expression was more common in GBM patients than ND. (**C**) Most plasma EVs expressed CD9 tetraspanin only. GBM patients had increased CD9+, CD9+/CD81+, CD9+/CD63+/CD81+ EVs. (**D-G**). Most CD45+, CD11b+, CD31+/CD41a+ and CD31+/CD41a- EV populations in ND only expressed the tetraspanin CD9 while GBM patients had increased frequencies of CD9+, CD9+/CD81+ and CD9+/CD63+/CD81+ EVs. (**H**) Strategy for tracing cell of origin for CD9+/Phalloidin- EVs. (**I**) No significant differences between GBM and ND CD45+ (leukocyte common antigen) and CD31+CD41a- (endothelial) plasma EVs. GBM patients had increased CD11b+/CD45- EVs (presumed myeloid origin) while ND had increased CD31+CD41a+ (platelet-derived) EVs. (**J**) Strikingly, most CD11b+ plasma EVs do not express CD45. This is distinct from myeloid cells which would typically be CD11b+/CD45+. *$p < 0.05$, **$p < 0.01$, ***$p < 0.001$, ****$p < 0.0001$.

vs 0.37%, $p = 0.005$) compared to normal donors (Figure 4B). Normal donor had increased expression of CD45+ EVs (mean 4.91% vs 13.67%, $p = 0.04$). Among the three EV-associated tetraspanins assessed, most plasma EVs expressed CD9 only (Figure 4C). GBM patients had increased CD9+ (mean 55.59% vs 24.33%, $p < 0.00001$), CD9+CD63+ (mean 3.84% vs 0.20%, $p = 0.04$), CD9+CD81+ (mean 5.90% vs 0.24%, $p = 0.003$) and CD9+CD63+CD81+ EVs (mean 0.84% vs 0.05%, $p = 0.007$). Most of the CD45+, CD11b+, CD31+CD41a+, and CD31+CD41a– EVs in normal donors were CD9+CD63-CD81–, while in GBM patients they could be CD9+, CD9+CD81+, or CD9+CD63+CD81+ (Figure 4D-G). Further gating of CD9+/phalloidin– EVs was performed to deduce their cells of origin (Figure 4H). GBM patients had increased CD11b+CD45– EVs (putative myeloid-derived EVs) compared to normal donors (mean 14.70% vs 3.9%, $p = 0.0008$) (Figure 4I).Interestingly, further gating of phalloidin-negative events based on CD45 and CD11b expression showed most positive events were single positives for either CD45 or CD11b (Figure 4J). Unlike CD11b+ myeloid cells which would be expected to be nearly universally positive for CD45 as well, very few double positive CD45+/CD11b+ EVs were seen. However, GBM patients again tended to have higher percentage of CD11b+CD45– EVs compared to normal donors (mean 10.37% vs 4.72%, $p = 0.25$), while normal donors tended to have higher percentage of CD45+CD11b– EVs (mean 4.95% vs 12.75%, $p = 0.05$).

Differentially Expressed EV Subpopulations in GBM Patients and Normal Donors

t-SNE analysis based on relative SSC, CD9, CD63, CD81, CD31, CD45, CD11b, and CD41a values on a data set combining 10 GBM patients and 10 normal donors (Figure 5A) revealed distinct clusters enriched in GBM patients and normal donors. GBM patients' plasma EVs had increased CD9, CD81, and CD11b expression (Supplementary Figure 7). FlowSOM revealed 15 distinct EV subpopulations (Figure 5B, C). Pop4 (mean 8.95% vs 0.17, $p < 0.0001$), Pop6 (mean 8.76% vs 0.11%, $p < 0.0001$), Pop7 (mean 2.08% vs 0.01%, $p < 0.0001$),Pop8 (mean 0.62% vs 0.003%, $p = 0.0003$), Pop10 (mean 0.21% vs 0.02%, $p = 0.0019$), and Pop11 (mean 0.13% vs 0.05%, $p = 0.01$) were enriched in GBM patients while Pop0 (mean 66.14% vs 79.67%, $p = 0.005$), Pop2 (mean 1.48% vs 5.02%, $p = 0.015$) were enriched in normal donors. No correlation was seen between enhancing tumor volume or total tumor volume and plasma EV subpopulations identified by multiparametric analysis. However, blinded analysis of a small independent cohort of 5 GBM patients and 5 normal donors using thresholds distinguishing GBM and ND in our earlier experiments based on CD9, CD81, population 8, and a combination of populations 0 and 6 correctly identified GBM or ND in all cases except CD81 in a single GBM case (Supplementary Figure 8).

Discussion

Plasma EVs are promising biomarkers in GBM patients. Plasma EV concentration may serve indicate tumor burden as GBM patients have higher plasma EV concentrations than healthy donors[17,21] and plasma EV decline after tumor resection and increase with relapse.[17,22] Those studies are based on bulk plasma EV analysis, without isolating tumor-derived EVs. Given that GBM-derived EVs can cross the blood–brain barrier,[23,24] GBM-derived EVs in plasma may also be a biomarker. Orally administered 5-aminolevulinic acid (5-ALA) in GBM patients produces fluorescent protoporphyrin IX (PpIX)-positive EVs which can be detected in plasma.[25,26] However, GBM-derived plasma EVs are very rare compared to nonneoplastic plasma EVs and show great individual variability.[27–30] This suggests they do not contribute significantly to the bulk changes seen in plasma EVs in GBM patients. Improved nanoparticle flow cytometry has allowed determining cell of origin for EV subpopulations.[31] Based on this, we hypothesized that characterizing abundant non-neoplastic plasma EVs by size (SSC), EV-associated tetraspanin (CD9/CD63/CD81), and parental cell marker (CD11b/CD31/CD41a/CD45) expression would reveal novel potential GBM biomarkers.

EV flow cytometry requires special technical considerations that we have addressed through the spectral acquisition parameters afforded by the Cytek Aurora flow cytometer. EVs are smaller and dimmer than cells, creating flow cytometry challenges. Many investigators address this by calibrating flow cytometry using microbeads.[22,26,28,32] Light side scatter approximates particle size when particles are smaller than the fluorescence wavelength. However, this is complicated by different refractory indices in calibrating microbeads and actual EVs.[33] Polystyrene beads have a higher refractory index (RI = 1.627) compared to silica beads (RI = 1.44) and produce more side scatter for a given size (Figure 1B). EVs' refractory index is like silica beads (core RI = 1.38), and side scatter (SSC) can approximate their size.[34] However, most particles detected by SSC in our study are not necessarily EVs. True EVs should express EV surface markers at levels > background. Because EVs vary in both size and surface marker expression, we only used SSC to gate on particles in an EV size range but not to determine the absolute number of EVs.

In addition, staining EVs for flow cytometry requires a different approach than staining cells to remove unbound fluorescent antibodies. Excess antibodies are easily removed from cells in suspension by brief centrifugation, but this would produce unacceptable reduction in EV yield. We found that size exclusion chromatography was an efficient method for removing unbound antibodies. This decreased EV yield but only to acceptable levels, in keeping with prior reports.[35,36] SEC separates particles based on size and removes many soluble proteins but does not specifically separate EVs from non-EVs. In our study, most of the particles in the EV size range after SEC purification did not express the EV-associated tetraspanin CD9 when acquisition was performed with an SSC-500 threshold, suggesting contamination with non-EV particles. Furthermore, lowering the EV detection size threshold significantly increased background noise. We therefore changed to a fluorescence-triggering threshold. Combining this with SEC purification minimized background noise, keeping false positive event rate below 10 events/s when collected at low speed (5 µl/min). Plasma has extremely high particle concentrations and requires dilution before flow cytometry

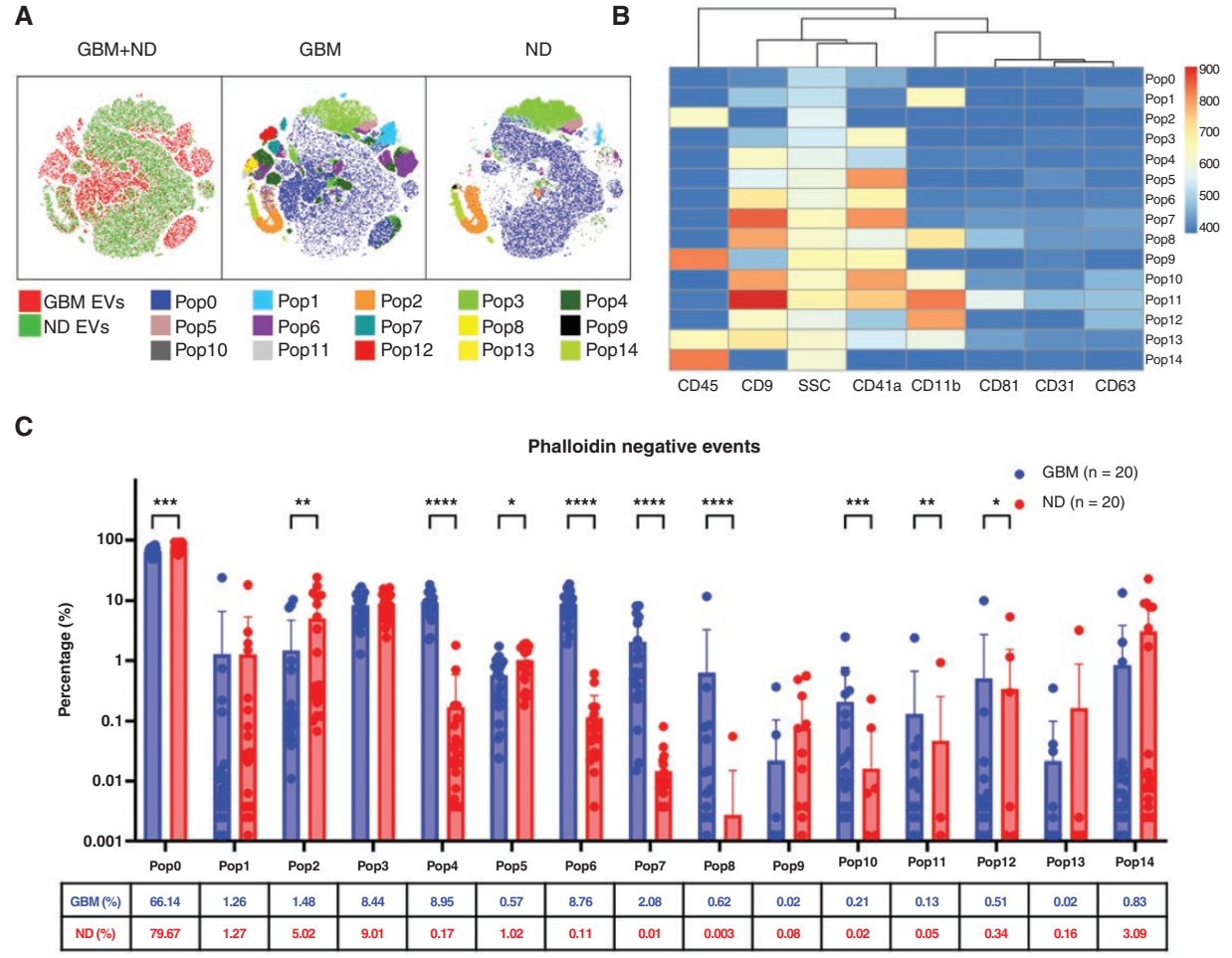

Figure 5 T-SNE and FlowSOM analysis reveal differently expressed plasma EV subpopulations in GBM and normal donors. (**A**) T-SNE (t-distributed stochastic neighbor embedding) analysis based on SSC, CD9, CD81, CD63, CD31, CD45, CD11b, and CD41a reveals different plasma EV clustering features for GBM patients and normal donors. (**B**) FlowSOM (self-organizing maps of flow cytometry data) analysis reveals 15 EV subpopulations differing in size (SSC) and surface marker expression. (**C**) Some groups are enriched in ND (Pop0, Pop2) while others are enriched in GBM (Pop4, Pop6, Pop7, Pop8, Pop10, Pop11). *$p < 0.05$, ***$p < 0.001$, ****$p < 0.0001$.

to avoid swarm effects. Prior studies suggest EVs can be gated by fluorescence labeling at 10^6–10^8 particles/ml and a 1:1000 dilution.[37] In our study, we did not observe any swarm effects at a 1:800 dilution. Having worked through these technical challenges for plasma EV staining and flow cytometry acquisition, we further minimized background noise and detection of non-EV populations by focusing on phalloidin-negative (ie actin-negative) events to exclude cell debris.

The EV-associated tetraspanins CD9, CD81, and CD63 are among the most widely studied surface markers for EV flow cytometry analysis.[28,38] An earlier study also found that CD9 is the most abundant plasma EV-associated tetraspanin in GBM patients[28] and that CD9+/CD81+ and CD9+/CD63+ plasma EVs are increased. CD9+ EVs represented up to 70% of detected tetraspanin+ EVs but the frequency of EVs expressing more than one tetraspanin was <5%. Our data are similar, showing that CD9 single-positive EVs are much more common than CD9+ EVs that also express CD63 or CD81 (Figure 4C). Nonneoplastic cell line-derived EVs have also been reported to have more homogeneous tetraspanin expression than GBM cell lines (CD9>CD81>>>CD63).[28] This is echoed in our plasma EV analysis (Figure 4D-G). Most EVs expressing nonneoplastic cell of origin markers in normal donors only express CD9 among the tetraspanins we examined while GBM patients have more heterogenous tetraspanin expression with increased CD9+CD81+ and CD9+CD63+CD81+ EVs.

Our data suggest EVs expressing the myeloid marker CD11b are increased in GBM patients (Figure 4I). These presumably originate from myeloid cells though, surprisingly, they do no express leukocyte common antigen (CD45). This does not represent general lack of staining for more than one surface marker as many also express CD9, CD63, and CD81. Rather, it seems likely that CD45 expression is not universal in myeloid-derived EVs (as opposed to myeloid cells). Regardless, increased myeloid-derived

EVs is unsurprising given known EV functions including modulating immune cells and myeloid cell-mediated systemic immunosuppression in GBM.[39] GBM EVs *in vitro* induce normal monocyte differentiation into myeloid-derived suppressor cells (MDSCs, HLADR-/CD11b+) that inhibit T cell proliferation.[40] GBMs are heavily infiltrated by monocytic cells and GBM patients have increased circulating MDSCs,[41,42] many of which originate from tumor-infiltrating monocytes.[43] This contributes to profound systemic immunosuppression with diminished peripheral T cell numbers and function and downregulation of major histocompatibility complex class II expression.[44] Given these findings, we speculate that differences in nonneoplastic plasma EVs in GBM patients compared to normal donors may primarily reflect EVs released by immunosuppressive monocytes, though the relative contribution of tumor-infiltrating versus circulating immunosuppressive monocytes remains to be determined. Though detailed interactions between GBM cells, GBM EVs, and host immune cell EVs *in situ* remain undefined, thymic involution and decreased T cell counts in GBM-bearing mice have been linked to nonsteroid soluble, high molecular weight (>100 kDa) factors in plasma potentially compatible with EVs.[45] These findings also suggest that combining plasma EV biomarkers with profiles of circulating immune cell populations might further increase the accuracy of liquid biopsy.

Finally, automated multiparametric t-SNE and FlowSOM analysis minimized bias from manual gating and expanded our findings. This confirmed our earlier analysis by demonstrating that GBM patients have increased CD9+CD11b+CD45– plasma EVs corresponding to Pop8/10/11 marked by high CD9 and CD11 expression in FlowSOM (Figure 5). Normal donors have increased CD45+ EVs corresponding to Pop 2 with high CD45 expression. Moreover, this automated approach directly visualized 15 different EV subpopulations in GBM and normal donor plasma. These findings support our hypothesis that bulk non-neoplastic plasma EV phenotypes in GBM patients are distinct from healthy donors. To the best of our knowledge, this is the first study to apply t-SNE and FlowSOM on EV flow data analysis. These parameters could be applied to predict tumor presence or absence prospectively in the future. Given our promising initial results and that flow cytometry is widely available and can produce results within a few hours, this technique seems feasible and promising for clinically applicable liquid biopsy in GBM that will need to be explored and validated in larger samples.

Supplementary material

Supplementary material is available online at *Neuro-Oncology Advances* online.

Keywords:

extracellular vesicles | flow cytometry | glioblastoma | liquid biopsy

Conflict of Interest:

no authors have relevant conflicts of interest to disclose.
Funding: Brains Together for a Cure Foundation, Mayo Clinic Department of Neurological Surgery

Authorship

Conceptualization and Design: A.A., C.F., I.F.P.
Data collection: A.A., C.F., L.C.G., A.W., S.M.B., M.M.J.B., M.Y.J., J.N.S.
Analysis: A.A., C.F., L.C.G., A.W., S.M.B., M.M.J.B., M.Y.J., A.J.J., I.F.P.
Drafting/ editing manuscript: A.A., C.F., L.C.G., A.W., S.M.B., M.M.J.B., M.Y.J., J.N.S., A.J.J., I.F.P.
Supervision: I.F.P.

References

1. Ostrom QT, Cioffi G, Gittleman H, et al. CBTRUS statistical report: primary brain and other central nervous system tumors diagnosed in the United States in 2012-2016. *Neuro Oncol.* 2019;21(Suppl 5):v1–v100.
2. Ostrom QT, Gittleman H, Stetson L, Virk S, Barnholtz-Sloan JS. Epidemiology of intracranial gliomas. *Prog Neurol Surg.* 2018;30:1–11.
3. Nam JY, de Groot JF. Treatment of glioblastoma. *J Oncol Pract.* 2017;13(10):629–638.
4. Marenco-Hillembrand L, Wijesekera O, Suarez-Meade P, et al. Trends in glioblastoma: outcomes over time and type of intervention: a systematic evidence based analysis. *J Neurooncol.* 2020;147(2):297–307.
5. Stupp R, Mason WP, van den Bent MJ, et al; European Organisation for Research and Treatment of Cancer Brain Tumor and Radiotherapy Groups. Radiotherapy plus concomitant and adjuvant temozolomide for glioblastoma. *N Engl J Med.* 2005;352(10):987–996.
6. Balana C, Capellades J, Pineda E, et al. Pseudoprogression as an adverse event of glioblastoma therapy. *Cancer Med-Us.* 2017;6(12):2858–2866.
7. Thust SC, van den Bent MJ, Smits M. Pseudoprogression of brain tumors. *J Magn Reson Imaging.* 2018;48(3):571–589.
8. Muller Bark J, Kulasinghe A, Chua B, Day BW, Punyadeera C. Circulating biomarkers in patients with glioblastoma. *Br J Cancer.* 2020;122(3):295–305.
9. Zaborowski MP, Balaj L, Breakefield XO, Lai CP. Extracellular vesicles: composition, biological relevance, and methods of study. *BioScience.* 2015;65(8):783–797.
10. Hallal S, Azimi A, Wei H, et al. A comprehensive proteomic SWATH-MS workflow for profiling blood extracellular vesicles: a new avenue for glioma tumour surveillance. *Int J Mol Sci.* 2020;21(13):4754.
11. Van der Mijn JC, Sol N, Mellema W, et al. Analysis of AKT and ERK1/2 protein kinases in extracellular vesicles isolated from blood of patients with cancer. *J Extracell Vesicles.* 2014; 3(1):25657.
12. Zottel A, Šamec N, Kump A, et al. Analysis of miR-9-5p, miR-124-3p, miR-21-5p, miR-138-5p, and miR-1-3p in glioblastoma cell lines and extracellular vesicles. *Int J Mol Sci.* 2020;21(22):8491.
13. Mallawaaratchy DM, Hallal S, Russell B, et al. Comprehensive proteome profiling of glioblastoma-derived extracellular vesicles identifies markers for more aggressive disease. *J Neurooncol.* 2017;131(2):233–244.

14. Ebrahimkhani S, Vafaee F, Hallal S, et al. Deep sequencing of circulating exosomal microRNA allows non-invasive glioblastoma diagnosis. *NPJ Precis Oncol*. 2018;2(1):28.
15. García-Romero N, Carrión-Navarro J, Esteban-Rubio S, et al. DNA sequences within glioma-derived extracellular vesicles can cross the intact blood-brain barrier and be detected in peripheral blood of patients. *Oncotarget*. 2017;8(1):1416–1428.
16. Huang M, Peng X, Yang L, et al. Non-coding RNA derived from extracellular vesicles in cancer immune escape: Biological functions and potential clinical applications. *Cancer Lett*. 2021;501:234–246.
17. Osti D, Del Bene M, Rappa G, et al. Clinical significance of extracellular vesicles in plasma from glioblastoma patients. *Clin Cancer Res*. 2019;25(1):266–276.
18. Welsh JA, Van Der Pol E, Arkesteijn GJA, et al. MIFlowCyt-EV: a framework for standardized reporting of extracellular vesicle flow cytometry experiments. *J Extracell Vesicles*. 2020;9(1):1713526.
19. Van Gassen S, Callebaut B, Van Helden MJ, et al. FlowSOM: Using self-organizing maps for visualization and interpretation of cytometry data. *Cytometry A*. 2015;87(7):636–645.
20. Fedorov A, Beichel R, Kalpathy-Cramer J, et al. 3D Slicer as an image computing platform for the quantitative imaging network. *Magn Reson Imaging*. 2012;30(9):1323–1341.
21. Cumba Garcia LM, Peterson TE, Cepeda MA, Johnson AJ, Parney IF. Isolation and analysis of plasma-derived exosomes in patients with glioma. *Front Oncol*. 2019;9:651.
22. Koch CJ, Lustig RA, Yang XY, et al. Microvesicles as a biomarker for tumor progression versus treatment effect in radiation/temozolomide-treated glioblastoma patients. *Transl Oncol*. 2014;7(6):752–758.
23. Treps L, Edmond S, Harford-Wright E, et al. Extracellular vesicle-transported Semaphorin3A promotes vascular permeability in glioblastoma. *Oncogene*. 2016;35(20):2615–2623.
24. Banks WA, Sharma P, Bullock KM, et al. Transport of extracellular vesicles across the blood-brain barrier: brain pharmacokinetics and effects of inflammation. *Int J Mol Sci* . 2020;21(12):4407.
25. Maas SLN, van Solinge TS, Schnoor R, et al. Orally administered 5-aminolevulinic acid for isolation and characterization of circulating tumor-derived extracellular vesicles in glioblastoma patients. *Cancers (Basel)*. 2020;12(11):3297.
26. Jones PS, Yekula A, Lansbury E, et al. Characterization of plasma-derived protoporphyrin-IX-positive extracellular vesicles following 5-ALA use in patients with malignant glioma. *EBioMedicine*. 2019;48:23–35.
27. Zeng A, Wei Z, Yan W, et al. Exosomal transfer of miR-151a enhances chemosensitivity to temozolomide in drug-resistant glioblastoma. *Cancer Lett*. 2018;436:10–21.
28. Ricklefs FL, Maire CL, Reimer R, et al. Imaging flow cytometry facilitates multiparametric characterization of extracellular vesicles in malignant brain tumours. *J Extracell Vesicles*. 2019;8(1):1588555.
29. Fraser K, Jo A, Giedt J, et al. Characterization of single microvesicles in plasma from glioblastoma patients. *Neuro Oncol*. 2019;21(5):606–615.
30. Sartori MT, Della Puppa A, Ballin A, et al. Circulating microparticles of glial origin and tissue factor bearing in high-grade glioma: a potential prothrombotic role. *Thromb Haemost*. 2013;110(2):378–385.
31. Marchisio M, Simeone P, Bologna G, et al. Flow cytometry analysis of circulating extracellular vesicle subtypes from fresh peripheral blood samples. *Int J Mol Sci* . 2020;22(1):48.
32. Nielsen MH, Beck-Nielsen H, Andersen MN, Handberg A. A flow cytometric method for characterization of circulating cell-derived microparticles in plasma. *J Extracell Vesicles*. 2014;3(1):10
33. van der Pol E, de Rond L, Coumans FAW, et al. Absolute sizing and label-free identification of extracellular vesicles by flow cytometry. *Nanomed Nanotechnol Biol Med*. 2018;14(3):801–810.
34. van der Pol E, van Leeuwen TG, Yan X. Misinterpretation of solid sphere equivalent refractive index measurements and smallest detectable diameters of extracellular vesicles by flow cytometry. *Sci Rep*. 2021;11(1):24151.
35. Anderboom PM, Dasari S, Ruegsegger GN, et al. A size-exclusion-based approach for purifying extracellular vesicles from human plasma. *Cell Rep Methods*. 2021;1(3):100055.
36. Tian Y, Gong M, Hu Y, et al. Quality and efficiency assessment of six extracellular vesicle isolation methods by nano-flow cytometry. *J Extracell Vesicles*. 2020;9(1):1697028.
37. Tertel T, Görgens A, Giebel B. Analysis of individual extracellular vesicles by imaging flow cytometry. *Methods Enzymol*. 2020;645:55–78.
38. Théry C, Witwer KW, Aikawa E, et al. Minimal information for studies of extracellular vesicles 2018 (MISEV2018): a position statement of the International Society for Extracellular Vesicles and update of the MISEV2014 guidelines. *Journal of Extracellular Vesicles*. 2018;7(1):1535750.
39. Benecke L, Coray M, Umbricht S, Chiang D, Figueiró F, Muller L.Exosomes: small EVs with large immunomodulatory effect in glioblastoma. *Int J Mol Sci* . 2021;22(7):3600.
40. Himes BT, Peterson TE, de Mooij T, et al. The role of extracellular vesicles and PD-L1 in glioblastoma-mediated immunosuppressive monocyte induction. *Neuro Oncol*. 2020;22(7):967–978.
41. Parney IF, Waldron JS, Parsa AT. Flow cytometry and in vitro analysis of human glioma-associated macrophages. Laboratory investigation. *J Neurosurg*. 2009;110(3):572–582.
42. Gustafson MP, Lin Y, New KC, et al. Systemic immune suppression in glioblastoma: the interplay between CD14+HLA-DRlo/neg monocytes, tumor factors, and dexamethasone. *Neuro Oncol*. 2010;12(7):631–644.
43. Chae M, Peterson TE, Balgeman A, et al. Increasing glioma-associated monocytes leads to increased intratumoral and systemic myeloid-derived suppressor cells in a murine model. *Neuro Oncol*. 2015;17(7):978–991.
44. Himes BT, Geiger PA, Ayasoufi K, Bhargav AG, Brown DA, Parney IF. Immunosuppression in glioblastoma: current understanding and therapeutic implications. *Front Oncol*. 2021;11:770561.
45. Ayasoufi K, Pfaller CK, Evgin L, et al. Brain cancer induces systemic immunosuppression through release of non-steroid soluble mediators. *Brain*. 2020;143(12):3629–3652.